Applied Surface Science 422 (2017) 838–846

Contents lists available at ScienceDirect

Applied Surface Science

journal homepage: www.elsevier.com/locate/apsusc

Non-alloy/alloy transitions in the Sn/Cu(001) system: An STM, LEED and DFT study

P. Machain, J.E. Gayone, J.D. Fuhr*, H. Ascolani

Centro Atómico Bariloche, CNEA, and CONICET, Av. E. Bustillo 9500, R8402AGP Bariloche, Argentina

ARTICLE INFO

Article history:
Received 22 December 2016
Received in revised form 19 May 2017
Accepted 23 May 2017
Available online 26 May 2017

Keywords:
Surface
Alloy
Transition
STM
LEED
DFT

ABSTRACT

We show that surface alloying during growth of Sn on Cu(001) is inhibited at temperatures below 170 K. We have studied the non-alloying surface structures that are formed starting from low Sn coverage up to 0.65 ML, finding two novel non-alloying surface reconstructions. They were investigated by scanning tunneling microscopy (STM) and low energy electron diffraction (LEED) experiments, and by density functional theory (DFT) calculations. Increasing the temperature, we found that the exchange process is activated at 200–240 K causing the transformation of the initial non-alloyed surface into the corresponding alloyed one. The five known reconstructions of the Sn/Cu(100) surface alloy in the studied Sn coverage range are recovered when starting from the low temperature non-alloying phases. We analyze the atomistic processes involved in the non-alloy/alloy transitions, using first-principles calculations of the energy landscape of the Sn/Cu(001) system.

1. Introduction

Metal-on-metal epitaxial growth affords the opportunity to control the structural, chemical, and electronic behavior of bimetallic surfaces. Besides the commonly observed ordered overlayers, bimetallic systems may form true surface substitutional alloys, which often lack any direct bulk analogue [1–4]. Metallic adsorbates on Cu surfaces have been widely investigated due to the potential applications, in particular the improvement of the performance in heterogeneous catalysis [5,6]. Recently, surface Sn alloying was found to drastically reduce the reactivity of the Cu(001) surface to carboxyl deprotonation [7], and to reduce the interaction of chiral amino-helicenes molecules with the substrate [8].

Understanding the atomistic processes involved in the formation of the surface alloy can help in controlling the structures and morphology of the surface. Not only the formation of a surface alloy depends on the coverage [9], but the deposition of the metallic adsorbates at low temperature (LT) can prevent surface alloying. Karakalos et al. studied the overlayer to surface alloy transition in the Sn/Ni(111) system as a function of temperature and initial Sn coverage [10]. More recently, by growing Sn on Cu(111) at 100 K, Liang et al. discovered two novel non-alloying surface reconstructions [11].

The large lattice mismatch between Sn and Cu (a_{Sn} is ∼10% greater than a_{Cu}) produces a series of ordered phases when Sn is deposited on Cu(001) at room temperature (RT). Several studies of this system using low energy electron diffraction (LEED), Auger electron spectroscopy, scanning tunneling microscopy (STM), and surface X-ray diffraction have identified five reconstructions for Sn coverages between ∼0.2 ML and 0.7 ML [12–18]. Up to 0.5 ML of Sn coverage, all Sn atoms occupy substitutional sites in the top substrate layer forming true surface-alloy reconstructions: antiphase domain p(2 × 2) at ∼0.2 ML, p(2 × 6) at 0.37 ML, c(4 × 8) at 0.4 ML, and $(3\sqrt{2} \times \sqrt{2})R45^\circ$ at 0.5 ML. At higher Sn coverages, part of the Sn atoms can only be incorporated as adatoms. This is the case of the c(4 × 4) reconstruction formed with 0.625 ML. Another reconstruction (4 3/−3 4) has been reported for higher Sn coverage, although annealing to 410 K was required [19].

In this work we first studied in depth the non-alloying surface structures formed when depositing Sn on Cu(001) at LT, for Sn coverages ranging from <0.1 ML up to 0.65 ML. We then increased the temperature, activating the exchange process, and we studied the formation of ordered phases already known at RT when starting from LT non-alloying structures. We also studied the processes involved in the non-alloy/alloy transitions with the aid of first-principles calculations of the energy landscape of the Sn/Cu(001) system.

* Corresponding author.
E-mail address: fuhr@cab.cnea.gov.ar (J.D. Fuhr).

http://dx.doi.org/10.1016/j.apsusc.2017.05.201
0169-4332/

2. Experimental and calculation methods

The experiments were carried out in a UHV system with a base pressure in the low 10^{-10} mbar range and equipped with a variable-temperature Scanning Tunneling Microscope (STM, Omicron VT25), a LEED optics, and a home-made sputtering gun.

The Cu(001) substrate (Mateck, orientation accuracy $\pm 0.1^{\circ}$) was prepared by repeated cycles of Ar^{+} at 1.5 keV bombardment and then annealing at 800 K until a (1×1) LEED pattern with sharp spots and low background was obtained. Sn was evaporated from a home-made Knudsen cell onto clean Cu(001) surfaces at a rate of 0.1 ML every 2.5 min approximately, as follows from the calibration obtained from the LEED patterns of the mentioned reconstructions of the system. The Knudsen cell was located in the preparation area of the chamber.

The preparations at LT were performed as follows. The substrate was cooled by means of the continuous-flow cryostat associated to the STM working with liquid N_2. Temperatures were measured by using a Si diode that is located close to the sample on the clamp of the cold finger. In thermal equilibrium, the sample temperature is estimated to be 15 K higher than the Si diode reading. This correction was considered all along this article. Once the sample reached the lowest temperature (~130 K, typically), it was disconnected from the cold finger and moved to the manipulator sample-holder to receive the Sn dosis. Finished the evaporation, the sample was again connected to the cold finger. The sample temperature was not measured during evaporations. In order to keep the sample within a LT range (<200 K), the dosing times were limited to 4 min at most.

All the STM images were taken in constant-current mode using electrochemically etched W tips. Filled-states images are those obtained with negative bias voltages.

First-principles electronic structure calculations were performed within the DFT framework using the Quantum-espresso plane-wave code [20]. We used the Perdew–Burke–Ernzerhof generalized gradient approximation (PBE-GGA)[21,22] and the projector augmented wave method with explicit semicore electrons. Residual forces on the atoms after geometric relaxation were smaller than 10^{-3} Ry/a_0. For the surface calculations we used the slab method, with six layers representing the surface and a vacuum size of 10 Å. The Sn adsorption and incorporation was calculated in a 5×5 surface supercell. Except for the two lower layers that were kept fixed at the bulk distance, all the atoms in the cell were allowed to relax. We used an energy cut-off of 50 Ry and Brillouin integrations were done using $3 \times 3 \times 1$ grid. We simulated STM images within the Tersoff–Hamann approximation [23] in the constant

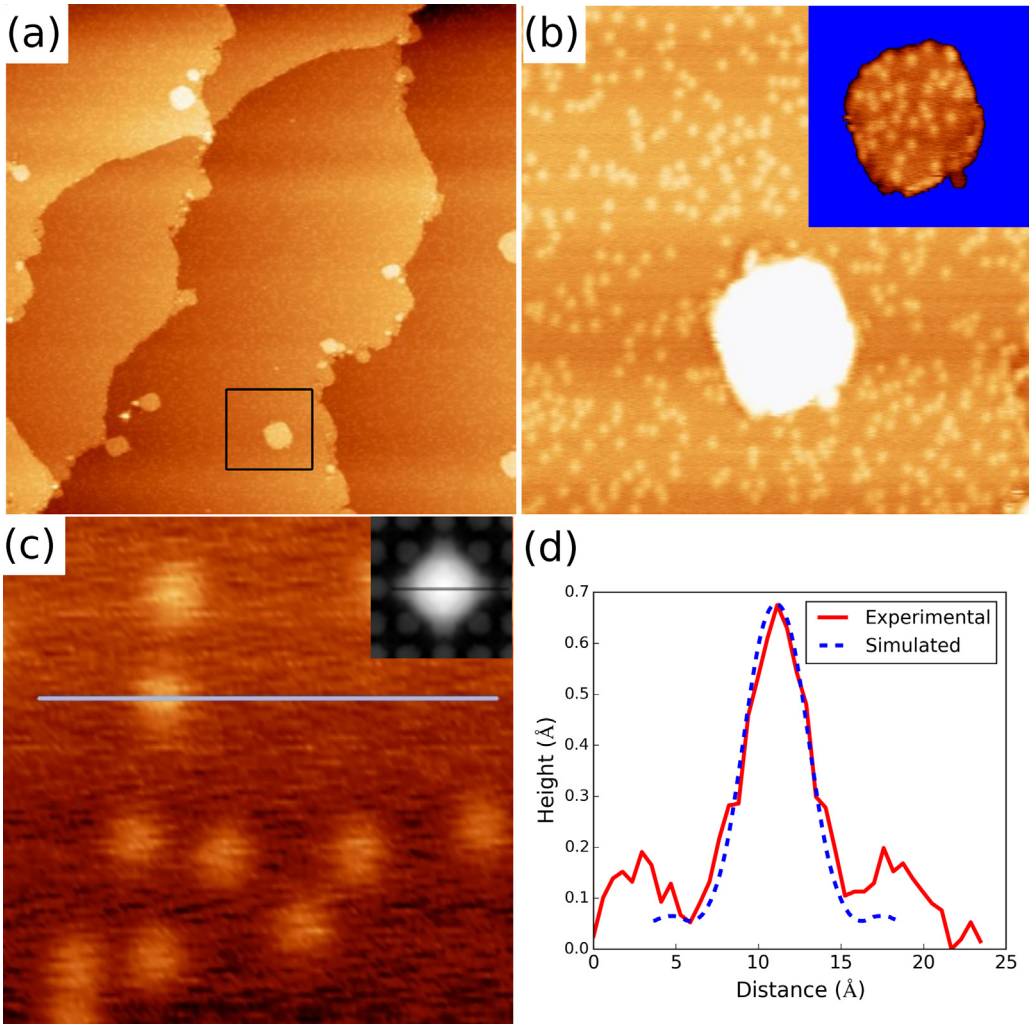

Fig. 1. Experimental STM images after evaporating 0.03 ML of Sn atoms at RT taken at 130 K with a bias voltage of −2 V and a reference current of 0.5 nA. (a) Filled-state image of 150 nm × 150 nm. (b) Zoom of a region of (a) including a island of one atomic-layer high (30 nm × 30 nm). As seen in the inset (12.8 nm × 12.8 nm), the island surface contains protrusions with a distribution identical to that observed on the terrace. (c) High resolution image showing individual spots corresponding to embedded Sn atoms, with a simulated STM image in the inset (6.15 nm × 6.15 nm). (d) Corrugation profile of the experimental image in panel (c), compared to a simulated STM profile. The simulated profile was obtained for the same bias voltage (−2 V) and an isodensity surface of 7×10^{-4} Å^{-3}; the height was rescaled for better comparison.

current mode, which corresponds to an isodensity surface of the integrated local density of states.

3. Results

3.1. Characteristics of the Sn/Cu(001) surface alloy

Fig. 1 shows STM images taken at 130 K of a surface prepared by depositing 0.03 ML of Sn atoms on a clean Cu(001) surface at RT. The time elapsed between the evaporation and the achievement of the lowest temperature was ∼30 min. A large scale image is presented in panel (a), showing large terraces separated by monoatomic steps. In addition, there are small islands with an average height of (1.9 ± 0.1) Å which were not present in the clean Cu(001) surface. Fig. 1(b) shows a detail of a zone with one of these islands, showing a homogeneous and disordered distribution of bright protrusions both on the terraces and on the island. The observed protrusions have an average height of (0.5 ± 0.1) Å and an average width of (4.2 ± 0.5) Å (Fig. 1(c) and (d)). These values are compatible with embedded Sn atoms, as follows from a comparison with the values reported in the literature for other similar surface alloys [24–26] and from a comparison with a simulated STM image for an isolated Sn embedded on the Cu(001) surface (Fig. 1(d)). Therefore, at very low coverages and RT, the Sn/Cu(001) system forms a homogeneous and disordered surface alloy.

A relevant issue related to the formation of a surface alloy is whether the deposited adatoms incorporate into the first surface layer in the terrace or at the steps. Typical examples of these cases are the In/Cu(001)[24] and the Pd/Cu(001) [25] systems: while In atoms incorporates at steps, Pd atoms do it on terraces. In the Sn/Cu(001) system, we observed that the mobility of the Sn atoms that are incorporated in the terrace is not high enough at RT to explain the homogeneous distribution obtained after the fast cooling procedure related to Fig. 1. In this sense, it is relevant to consider that the mobility of incorporated Sn atoms is negligible at 240 K, as we shall see below. We can therefore exclude that they were incorporated in the steps and only then spread uniformly throughout the first layer. We conclude that in the Sn/Cu(001) system the Sn adatoms incorporate in the terrace.

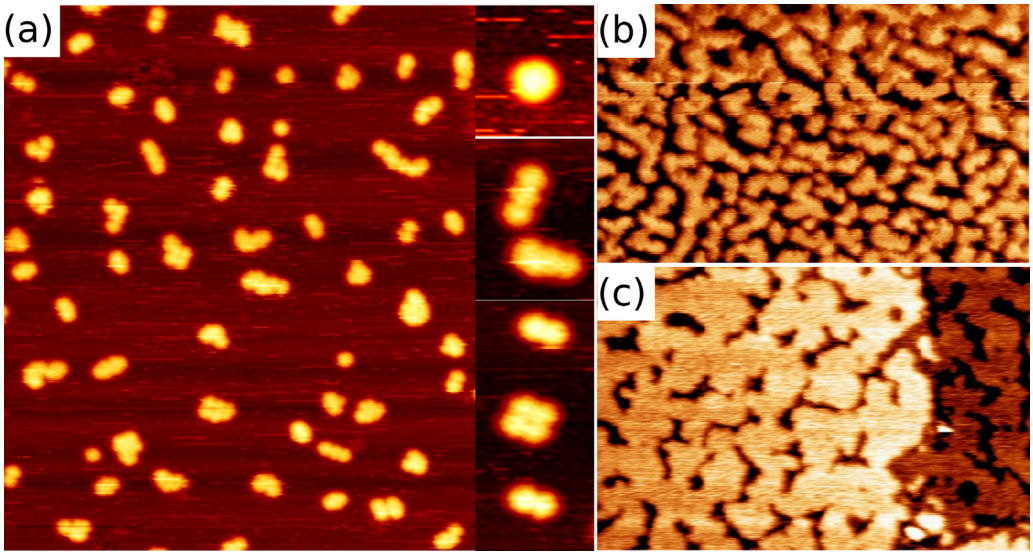

Fig. 2. Low temperature structures obtained for several Sn coverages on Cu(001). (a) STM image for 0.02 ML of Sn, showing protrusions of ∼12 Å width corresponding to clusters of 4 Sn adatoms. These clusters join to form dimers, trimers, quadruplets and larger agglomerates. The inset shows close-up images of the mentioned clusters. Image size: 39 nm × 45.1 nm; tunneling conditions: −0.9 V/0.5 nA. (b) STM image for 0.17 ML of Sn, where the islands have the same characteristics but are larger (80 nm × 48 nm); −0.2 V/1 nA. (c) STM image for 0.5 ML of Sn, showing the coalescence of the islands (80 nm × 53 nm); −0.1 V/0.8 nA.

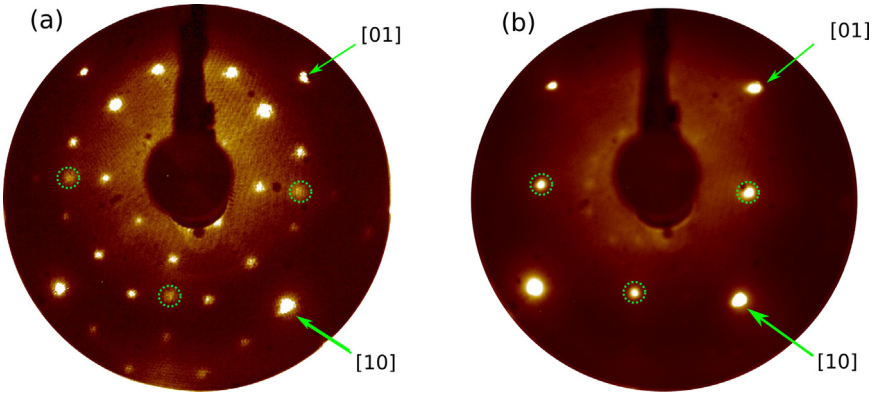

Fig. 3. LEED patterns of the two new ordered phases found at low temperatures. Both of them were measured at 130 K at 74 eV. (a) Representative diffraction pattern observed between 0.2 and 0.5 ML of Sn coverage (the shown one corresponds to 0.4 ML). It is composed of an intense 3 × 3 pattern plus the four spots at positions ±1/2 (indicated by green circles). (b) Representative $(4\sqrt{2} \times 2\sqrt{2})R45^{\circ}$ diffraction pattern corresponding to 0.65 ML of Sn coverage (green circles indicate ±1/2 spots). (For interpretation of the references to color in this figure legend, the reader is referred to the web version of this article.)

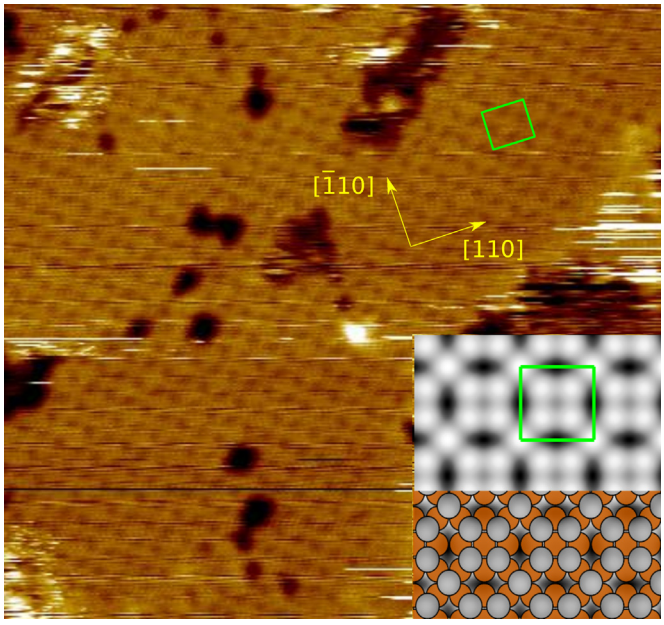

Fig. 4. High resolution STM images of the LT structure obtained for 0.5 ML Sn coverage on Cu(001). The green square indicates the unit cell of a 3×3 structure, with two inequivalent protrusions per unit cell. Image size: 19.7 nm × 18.4 nm; tunneling condition: −0.2 V/1 nA. Inset: Atomic structure from DFT calculation with simulated STM image (bias voltage of −0.2 V and isodensity surface of 7×10^{-4} Å^{-3}). (For interpretation of the references to color in this figure legend, the reader is referred to the web version of this article.)

3.2. Non-alloyed low-temperature structures

We deposited 0.02 ML of Sn atoms on the substrate held at LT following the procedure indicated in the experimental methods section. Fig. 2(a) shows a STM image taken at 130 K, where the surface is homogeneously covered by small islands of (2.0 ± 0.1) Å height, and no protrusions with the characteristics determined for embedded Sn atoms were detected. These observations show that the maximum temperature of the sample during its preparation was low enough to cause a reduction of the frequency of the direct-exchange events to undetectable values. Therefore, the observed islands must be composed of Sn adatoms alone. A close inspection of the islands indicates the existence of an internal structure. There are dots, dimers (composed of two dots), trimers, tetramers, etc. Zoomed images of these structures are shown in the inset of Fig. 2(a). The dots show a full-width half maximum (FWHM) of (12 ± 1) Å, which corresponds to an area of ∼110 Å^2. On the other hand, from the evaporator flux (determined by counting protrusions in the images of Fig. 1), the evaporation time, and the surface covered by the islands, an effective area of 25 Å^2 was obtained for each Sn adatom. Therefore, the observed dots are not single Sn adatoms but clusters of (4 ± 1) Sn adatoms.

We then investigated the phases of the non-alloyed Sn/Cu(001) interface as a function of the Sn-coverage up to ∼0.65 ML, monitoring the formed structures by STM and LEED. We started with a deposition of 0.17 ML of Sn. Fig. 2(b) shows a representative STM image of the obtained surface. It can be seen that the substrate is covered by a distribution of islands with the same characteristics, but larger, as those obtained for low coverage. With increasing Sn coverage, the clusters of Sn adatoms observed at 0.17 ML coalesce forming flat islands of monoatomic height, whereas the size of the observed pits is systematically reduced. This is illustrated in Fig. 2(c) by a representative STM image of the surface obtained with Sn coverages of 0.4 ML. We note that the depth of the pits is 2 Å, in concordance with the height of the initial islands.

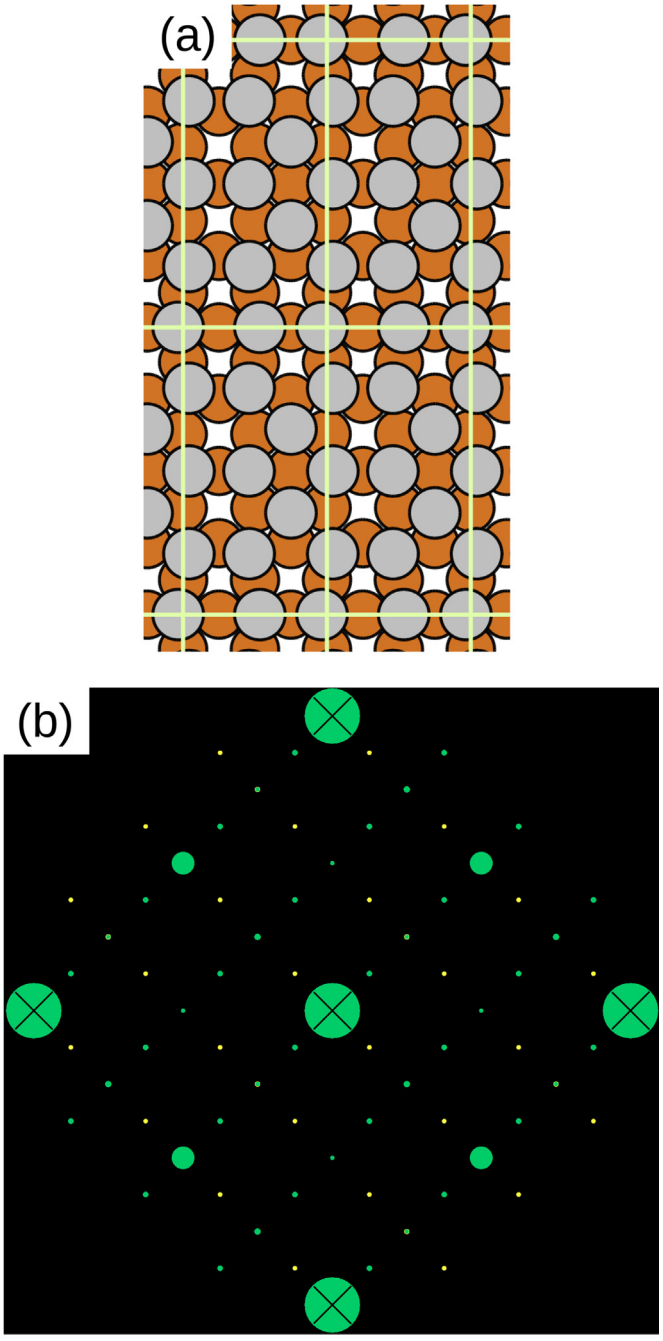

Fig. 5. (a) Tentative model for the $(4\sqrt{2} \times 2\sqrt{2})R45^\circ$ structure with 0.625 ML of Sn coverage, after relaxation with a DFT calculation. (b) Simulated $(4\sqrt{2} \times 2\sqrt{2})R45^\circ$ LEED pattern using a simple kinematical theory for a single layer of Sn adatoms. Crossed circles indicate 1×1 spots. Yellow and green spots corresponds to the two independent domains. The size of the spots is proportional to their intensity. (For interpretation of the references to color in this figure legend, the reader is referred to the web version of this article.)

Contrary to the rather disordered appearance of the surface observed at a mesoscopic level, the LEED clearly indicates that two different ordered phases are formed at low temperatures in the range between 0.2 and 0.65 ML of Sn coverage. Starting from low coverage, the LEED pattern shown in Fig. 3(a) arises at 0.2 ML, where faint but clear spots were observed, becoming sharp and intense between 0.3 and 0.5 ML. It is composed of an intense 3×3 pattern plus extra spots at the positions $(\pm 1/2, \pm 1/2)$ (indicated with green circles). In turn, at 0.65 ML, there is an abrupt change and the diffraction pattern shown in Fig. 3(b) is observed. From

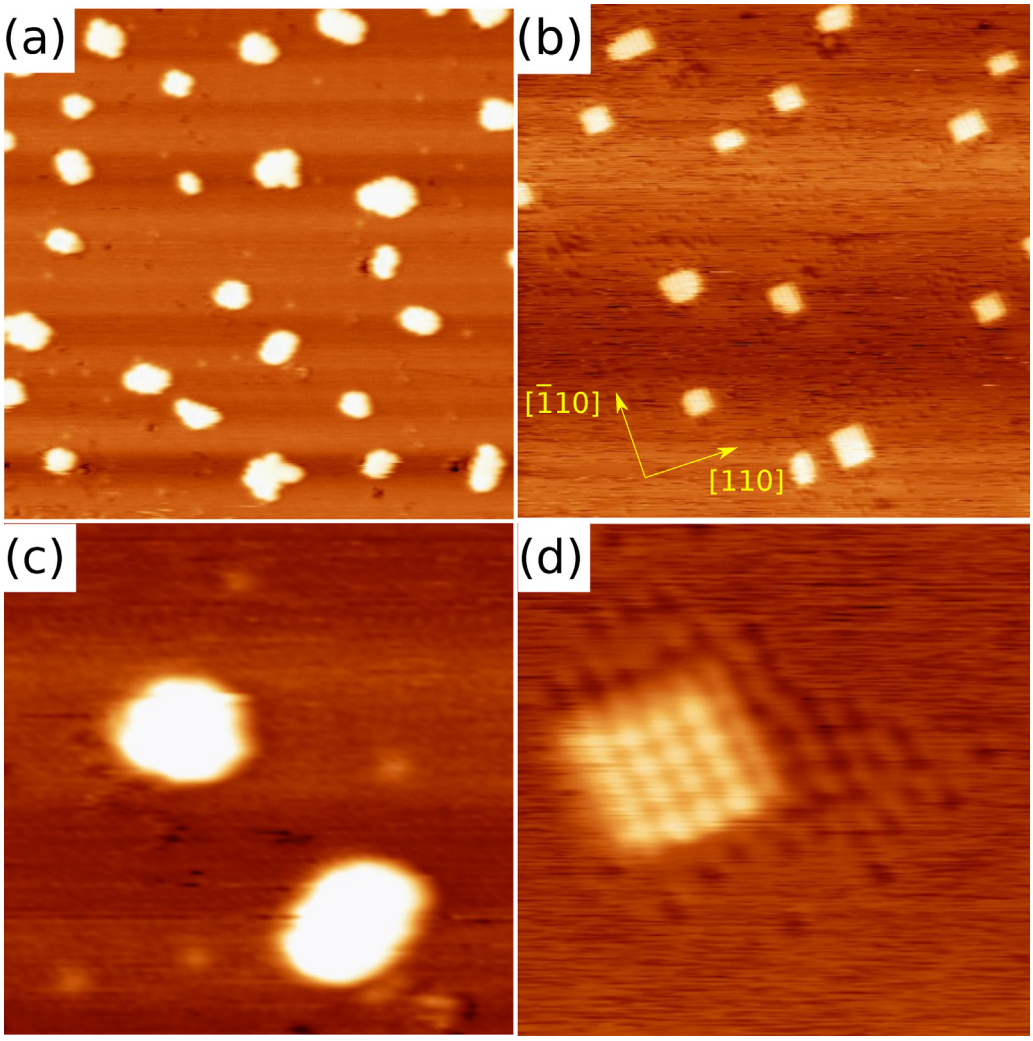

Fig. 6. STM images obtained for the same Sn coverage of Fig. 2(a) after increasing the sample temperature. (a) Image obtained with the sample at 200 K. Image size: 45.3 nm × 45.3 nm; Tunneling conditions: −1 V/0.5 nA. (b) Image obtained with the sample at 240 K. Size: 50 nm × 50 nm; conditions: −0.5 V/0.6 nA. (c) Zoom of image (a). Image size: (12.5 nm × 12.5 nm) (d) High resolution image showing a squared island composed of 16 protrusions (associated to Sn adatoms) arranged in a 2 × 2 structure. The island is surrounded by embedded Sn atoms. Image size: 9.1 nm × 9.1 nm; tunneling conditions: 0.5 V/0.6 nA.

a detailed analysis of the latter pattern and others taken at different energies, we conclude that it corresponds to a $(4\sqrt{2} \times 2\sqrt{2})R45^\circ$ structure. Similarly, by analyzing the pattern in Fig. 3(a) at different electron energies, we determined the following facts: (i) the only additional spots to the 3 × 3 pattern are those at the positions (±1/2, ±1/2); and (ii) the intensities of the observed (±1/2, ±1/2) spots are qualitatively consistent with those of the (±1/2, ±1/2) spots of the $(4\sqrt{2} \times 2\sqrt{2})R45^\circ$ pattern. Moreover, the intensity of the (±1/2, ±1/2) spots relative to the intensity of the (1/3, −1/3) spot of the 3 × 3 pattern increases with increasing Sn coverage. We therefore conclude that the diffraction pattern of Fig. 3(a) reflects the coexistence of a 3 × 3 phase (dominant) with the $(4\sqrt{2} \times 2\sqrt{2})R45^\circ$ one.

The high resolution STM image in Fig. 4 corresponds to a Sn coverage of 0.5 ML and shows some regions with inequivalent protrusions. The structure obtained from this STM image is compatible with a (3 × 3) unit cell with two inequivalent protrusions per unit cell, in agreement with our interpretation of the LEED pattern of Fig. 3(a). The inset in Fig. 4 shows an atomistic model for this (3 × 3) phase in which the coverage is 5/9 ML, together with a simulated STM image obtained by DFT calculations. The proposed model consists of Sn quadruplets linked by single Sn adatoms. As the resolution of the STM experiments is not enough to solve the internal structure of the quadruplets, we attribute them to the larger protrusions and the linking of Sn atoms to the smaller one. Remarkably, these Sn quadruplets can be related to the observed dots for low coverage (Fig. 2(a)).

Regarding the $(4\sqrt{2} \times 2\sqrt{2})R45^\circ$ phase, a characteristic of its LEED pattern, in the investigated energy range (50–130 eV), is that the (1/2) spots are approximately one order of magnitude more intense than the other fractionary spots. In addition, this phase transforms into the c(4 × 4) alloyed one when the temperature reaches RT and, hence, it is reasonable to assume that they have the same Sn coverage. According to a previously reported LEED study, the coverage of the c(4 × 4) phase is (0.625 ML). We therefore propose the following tentative model for the $(4\sqrt{2} \times 2\sqrt{2})R45^\circ$ phase: a c(2 × 2) structure with 2 extra Sn atoms allocated in such a way that a local 1 × 1 structure is formed, as illustrated in Fig. 5(a). Measurement of high-resolution STM images was extremely difficult in this case and we could not obtain any one to compare with the proposed model. To assess the plausibility of this model we have simulated the relative intensities of the "extra" LEED beams using a simple kinematical theory for a single layer of Sn adatoms, treating each atom as an isotropic scatterer [27]. The obtained simulated LEED pattern shown in Fig. 5(b) reproduces the main features of the experimental one (Fig. 3(b)), in particular the higher intensity of the (1/2) spots.

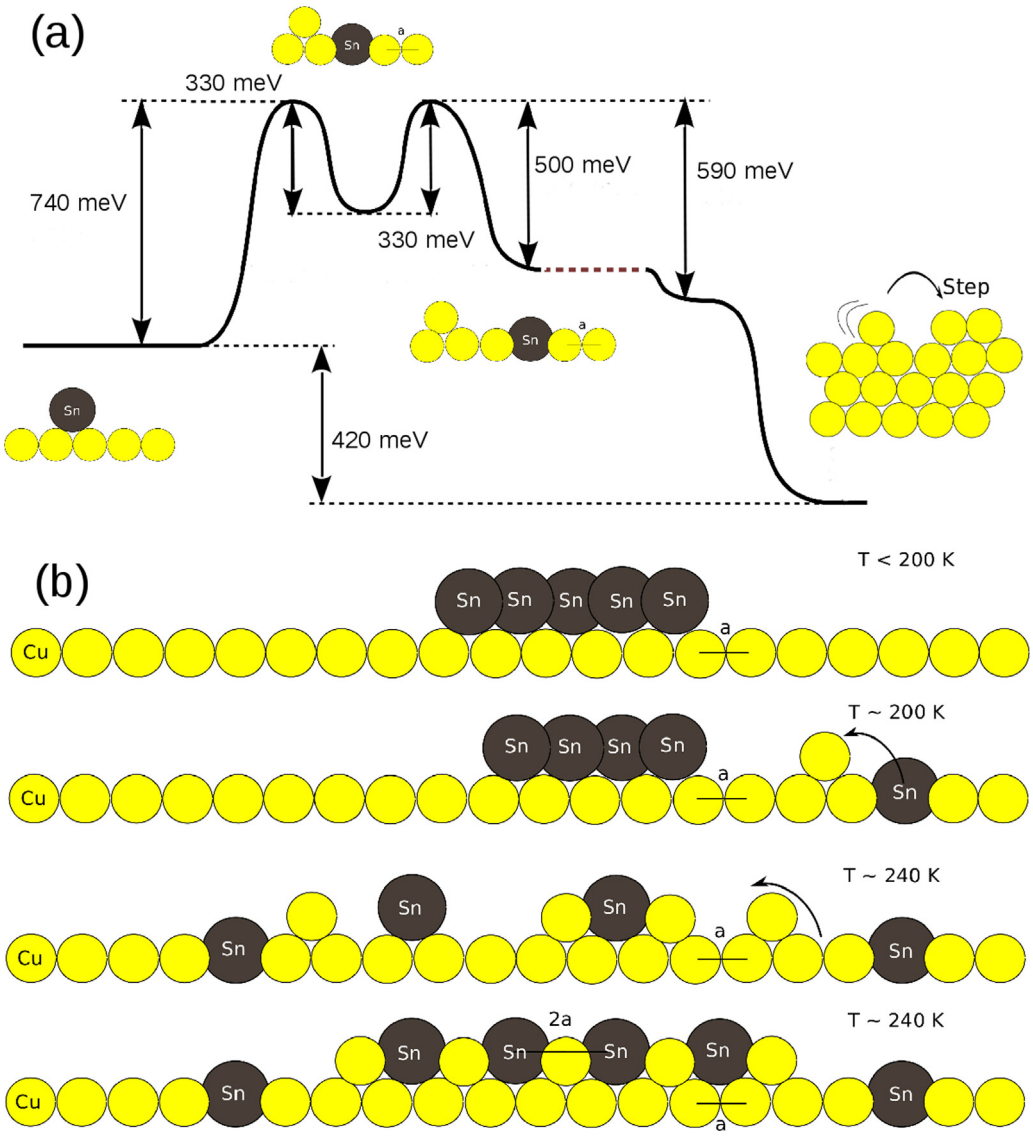

Fig. 7. (a) Energies and barriers, as calculated by DFT, of some atomistic mechanisms involved in the incorporation of the Sn atoms into the surface. (b) Processes involved in the non-alloy/alloy transition.

3.3. *Non-alloy/alloy transition followed by STM*

Next, we studied the transition from the non-alloyed structures obtained at low temperature, shown in the previous section, to the alloyed structures observed at RT. In order to estimate the temperature at which the exchange process is activated, we started from the same low coverage of Fig. 2(a), and performed several STM experiments increasing the temperature. Fig. 6(a) shows the STM image of a sample prepared at low temperature and then heated to ~200 K (the image was taken at this temperature). The main effect caused by increasing the sample temperature to 200 K is an increment of the size of the islands, and the appearance, in the regions between the islands, of protrusions with the characteristics of those produced by embedded Sn atoms. Therefore, at 200 K the exchange process is already activated but with low probability. Fig. 6(b) shows an STM image of the surface after increasing the temperature to 240 K. Important changes are observed in comparison with the image in panel (a), in particular there is a notorious change of the island shape from amorphous to rectangular. The changes undergone by the surface due to the increase of the temperature from 200 to 240 K are even more evident in Fig. 6(c) and (d). Very interestingly, the rectangular islands obtained at 240 K present a well-defined internal structure. In particular, the squared island observed in Fig. 6(d) contains 16 protrusions arranged in a 4×4 array, with an arrangement corresponding to a 2×2 structure. Note that there is a significant density of embedded Sn atoms in the region close to the island border which is not observed at 200 K. We also note that, although the formed rectangular islands have a distribution of sizes and shapes (see Fig. 6(b)), it is quite narrow. In fact, from the analysis of this and other similar images, it follows that the vast majority of islands are smaller than arrays of 6×6 protrusions. As diffusion of embedded Sn atoms was found to be highly unlikely at this temperature (around one event in 10 min), the positions of the embedded atoms reveal the site were the exchange events occurred. The fact that the embedded Sn atoms are not distributed homogeneously on the surface but localized around the rectangular islands strongly suggests that these islands form from the initial islands of Sn adatoms when the exchange process is activated.

In order to gain a deeper insight of the atomistic mechanisms involved in the incorporation of the Sn atoms into the surface, we obtained by DFT calculations some relevant energies and barriers involved in the process. Fig. 7(a) shows schematically the main

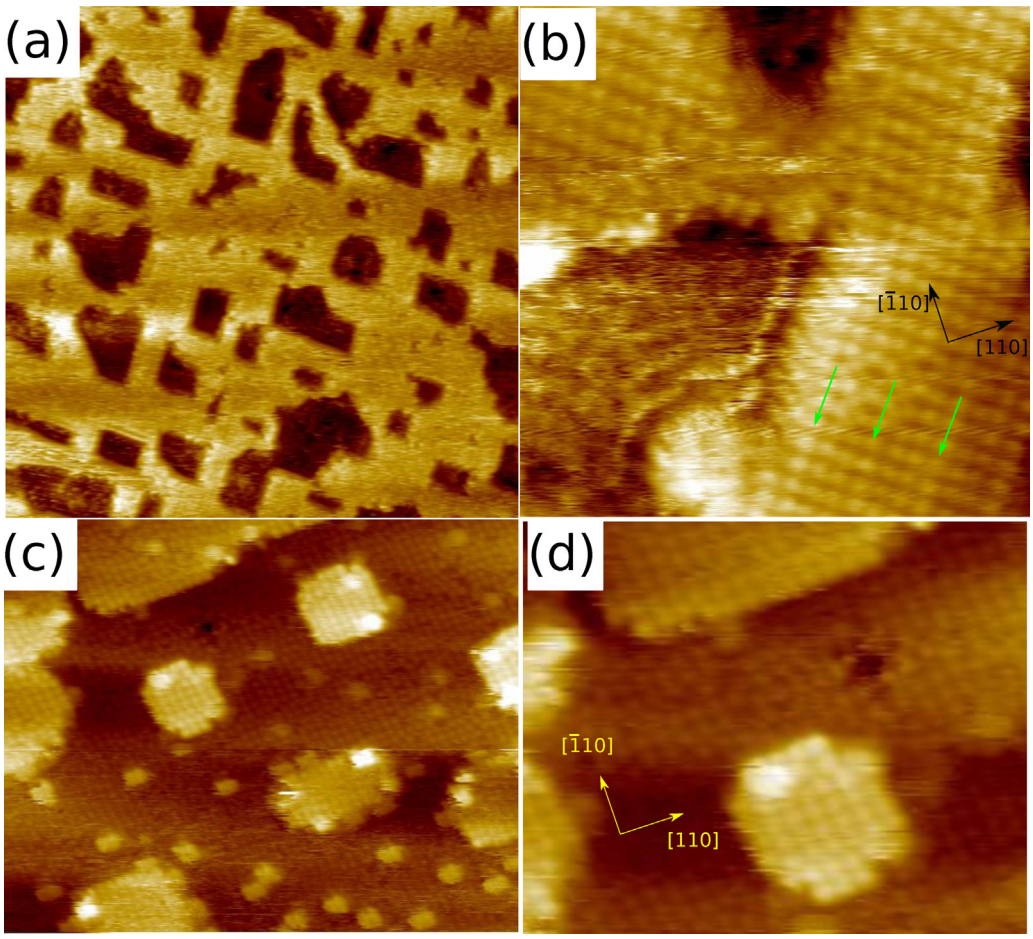

Fig. 8. STM images obtained after increasing the sample temperature for the cases of 0.5 and 0.17 ML of Sn coverage. (a) and (b) starting from the LT surface presented in Fig. 2(c) and increasing the temperature to 240 K. The arrows in panel (b) point to rows of brighter atoms, a sign of the $(3\sqrt{2} \times \sqrt{2})R45^{\circ}$ reconstruction. (c) and (d) starting from the LT structure presented in Fig. 2(b) and increasing the temperature to 255 K. Image sizes and tunneling conditions: (a) (50 nm × 50 nm) and −0.05 V/0.5 nA; (b) (10 nm × 10 nm) and −0.2 V/1.8 nA; (c) (30 nm × 24 nm) and −2.3 V/1 nA; (d) (13.6 nm × 11.2 nm) and −2.3 V/1 nA.

results. Starting from a Sn atom adsorbed on the Cu(001) surface, the energy barrier for a direct exchange process on a terrace is 740 meV, resulting in a Cu adatom as first-neighbour of the incorporated Sn atom with an energy 410 meV higher than the starting point. From this configuration the Cu adatom has two possibilities: it can either come back to the initial configuration (inverse exchange process) with an energy barrier of 330 meV, or it can diffuse to a second-neighbour site with an almost equal (within the calculation precision) energy barrier of 330 meV. From the second-neighbour sites, the diffusion of the Cu adatom is more probable, since there are multiple nearest-neighbors sites with similar diffusion barriers (around 500 meV). In turn, the diffusion for an isolated Cu adatom is 590 meV. Thereafter, the Cu adatom can eventually incorporate to the bulk Cu (for instance, through a surface step) attaining its cohesive energy, and resulting in a net gain of 420 meV with respect to the initial adsorbed Sn atom.

From the experimental STM images the main effect caused by increasing the sample temperature to 200 K is an increment of the size of the islands. Therefore, we can conclude that at 200 K it is the detachment of the Sn atoms from the formed islands that is activated. In turn, at 240 K the STM images show that all Sn atoms are incorporated as a surface alloy and therefore the exchange process must be activated at this temperature. However, from the calculated barrier, the incorporation should have a very low probability at this temperature. Indeed, considering a reasonable prefactor of 10^{13} Hz for the exchange event, the calculated barrier of 740 meV would result in a very low rate (∼0.003 Hz). Moreover, the Sn direct exchange process on a terrace competes with the Sn adatom diffusion, which have a DFT calculated energy barrier of 540 meV. The lower barrier, by 200 meV, for diffusion means that at 200 K the Sn adatom would make, on average, of the order of 10^5 diffusion hoppings before an exchange process (assuming equal prefactors for both processes). Therefore, the Sn adatom would travel several hundreds of lattice parameters before being incorporated, with a high probability of being attached to an island instead. In contrast, the STM images show that the Sn atoms embedded in the terrace are located mainly near the rectangular islands, and we can therefore conclude that there is a mechanism for incorporation near the islands with a barrier significantly lower than on the terrace. On the other hand, from the calculated barriers at RT the Sn adatoms will travel, on average, only some tens of lattice parameters before an exchange process. This is consistent with the conclusion that at RT there is a high probability of being incorporated in the terrace before attaining an step.

The picture in Fig. 7(b) synthesizes our understanding of the processes involved in the transition from the structure of Fig. 2(a) to the one in Fig. 6(b). At LT the exchange process is inhibited and we see the presence of islands mainly composed of adsorbed Sn quadruplets. At ∼200 K, the detachment from the formed islands is activated. As the exchange process at this temperature has a much lower probability than diffusion, we see a change in the morphology of the islands with only a very small quantity of embedded Sn atoms. At ∼240 K the exchange process is important but, as discussed above, only near the islands. In fact, all Sn atoms are part

of an alloy, with some of them forming characteristics rectangular islands with an internal structure corresponding to a 2×2 structure. These alloy islands are formed from pre-existing Sn islands and Cu atoms expelled from the topmost substrate layer as a consequence of a exchange process produced near the island.

To extend the STM study of the non-alloy/alloy transition to higher Sn coverages, we studied in detail two particular cases: 0.5 ML corresponding to the $(3\sqrt{2} \times \sqrt{2})R45^\circ$ reconstruction seen at RT, and 0.17 ML which is close to the starting coverage (0.2 ML) of the p(2 × 2) reconstruction [13]. Starting from the LT structure for 0.5 ML of Sn (Fig. 2(c)) we increased the temperature to 190 K. Although the aspect of the surface changed, the lack of well defined geometrical features still remains. In turn, at 240 K there is a qualitative transformation of the surface morphology. As seen in Fig. 8(a), the surface now presents two well-defined height levels separated by 2 Å and straight steps. In the high-resolution image shown in Fig. 8(b), a local $(\sqrt{2} \times \sqrt{2})R45^\circ$ atomic arrangement is observed on the islands. Moreover, in several regions of this image, the atomic arrangement corresponds to a $(3\sqrt{2} \times \sqrt{2})R45^\circ$ reconstruction, as one over three rows of Sn atoms has a higher apparent height. This is specially clear at the bottom-right region of the image. On the other hand, Fig. 8(c) and (d) show STM images of the obtained surface when, starting from the LT surface presented in Fig. 2(b), the sample temperature was increased to 255 K. In this case, the surface (both islands and terraces) is almost fully covered by protrusions arranged mostly in a defective (2 × 2) structure. In particular, several antiphase (2 × 2) domains, similar to those observed in the p(2 × 2) reconstruction [13], can be observed in the of Fig. 8(d). This indicates that the p(2 × 2) surface-alloy reconstruction is in the process of formation, although at this coverage there is no long range order and no LEED pattern can yet be seen. We can also recognize the 4 × 4 island of Fig. 6(b) as a precussor of this phase.

3.4. Non-alloy/alloy transition followed by LEED

We followed by LEED the non-alloy/alloy transition in four cases that cover the range of Sn coverages where well ordered alloyed phases are formed at RT. The chosen Sn coverages were those which at RT give rise to the following reconstructions of the system: p(2 × 6) (0.33 ML), c(4 × 8) (0.40 ML), $(3\sqrt{2} \times \sqrt{2})R45^\circ$ (0.50 ML), and c(4 × 4) (0.625 ML). See the schematic phase diagram depicted in Fig. 9(a). It is worthwhile recalling here that the passing from 0.5 to 0.625 ML brings a significant change in the structures observed at RT: while up to 0.5 ML of coverage all Sn atoms occupy substitutional sites in the top substrate layer, the c(4 × 4) reconstruction at 0.625 ML contains both substitutional and adsorbed Sn atoms.

After depositing Sn at LT (<170 K), sharp LEED patterns equivalent to the (3 × 3) shown in Fig. 9(a) were obtained in connection with the p(2 × 6), c(4 × 8) and $(3\sqrt{2} \times \sqrt{2})R45^\circ$ alloyed reconstructions. In turn, the $(4\sqrt{2} \times 2\sqrt{2})R45^\circ$ pattern presented in Fig. 9(b) was obtained for the c(4 × 4) reconstruction coverage. In each case, the evolution of the initial LEED pattern during the thermalization process (the sample holder of the manipulator was at RT) was continuously monitored as a function of time. The experiment ended when the pattern of the corresponding surface-alloy reconstruction became intense. The evolutions of the LEED patterns with time (increasing temperature) were similar in the four analyzed cases, as seen in the graphs of Fig. 9(b) and (c) corresponding to the cases of 0.33 ML and 0.625 ML, respectively. For each case, we followed the intensities of two spots, one corresponding to the initial non-alloyed phase and the other one corresponding to the final alloyed phase [28]. Looking at the 0.33 ML case (Fig. 9(b)), we see that approximately at 9 min after the moment when the samples were disconnected from the cold finger, the intensity of the 3 × 3 diffraction pattern started to rapidly decrease. At around

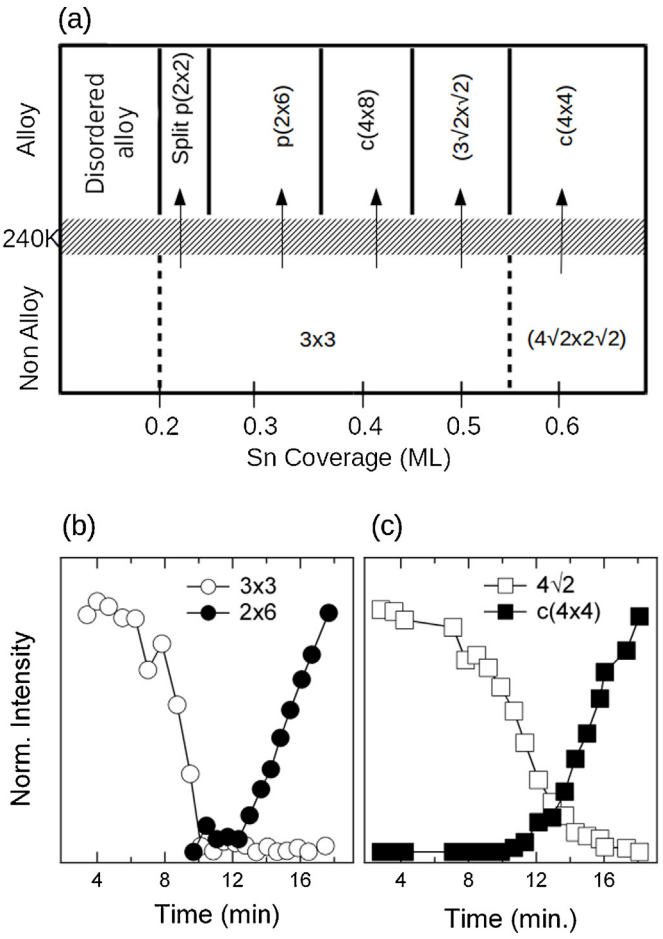

Fig. 9. (a) Schematic phase diagram of the Sn/Cu(100) system for temperatures between ~150 K and RT, and for Sn coverages between <0.1 and 0.65 ML. (b) Evolution with time of representative LEED spots for 0.33 ML of Sn. Empty circles: intensity of the (−2/3, −1/3) spot of the (3 × 3) pattern measured at 74 eV; Filled circles: intensity of the (−1/2, −1/2) spot of the p(2 × 6) RT reconstruction measured at 122 eV. (c) Evolution with time of representative LEED spots for 0.625 ML of Sn. Empty squares: intensity of the (−1/8, −5/8) spot of the $(4\sqrt{2} \times 2\sqrt{2})R45^\circ$ pattern measured at 122 eV; Filled squares: intensity of the (−1/3, −3/4) spot of the c(4 × 4) RT reconstruction measured at 122 eV.

11 min, the non-alloyed 3 × 3 phase completely disappeared from the LEED optics while, at the same time, the p(2 × 6) diffraction pattern started to develop. In the case of the 0.65 ML case, the general evolutions of the corresponding LEED patterns are similar to the previous case although the decreasing of the $(4\sqrt{2} \times 2\sqrt{2})R45^\circ$ would be slower.

These LEED results clearly show that, for all coverages, the same alloyed phases obtained when depositing at RT are recovered. Moreover, no intermediate phases are observed between the described LT phases and the RT phases. Last but no least, these results confirm that the non-alloy/alloy transition begins at about the same temperature (which from STM experiments is in the 200–240 K range) independently of the Sn coverage.

4. Conclusions

The deposited Sn atoms on the Cu(001) surface at RT are incorporated as substitutional atoms. Based on the experimental STM images at low coverage (0.03 ML) and DFT calculations, we conclude that the Sn atoms should incorporate in the terraces. On the other hand, depositing Sn on the Cu(001) surface at temperatures below 170 K deactivates the exchange process, inhibiting the formation of a surface alloy. Within this condition we found

two novel non-alloying surface reconstructions: a (3×3) structure and a $(4\sqrt{2} \times 2\sqrt{2})R45^{\circ}$ one. In the range of 0.2–0.5 ML of Sn coverage, the LEED patterns indicate that the two phases coexist on the surface, being the (3×3) structure the dominant one. In turn, at a coverage of 0.625 ML a pure $(4\sqrt{2} \times 2\sqrt{2})R45^{\circ}$ pattern is observed. We proposed an atomistic model for the (3×3) phase, obtained from high resolution STM images and DFT calculations, composed of Sn quadruplets linked by individual Sn adatoms. The fact that this (3×3) structure is the dominant phase along a wide ranges of coverages suggests that the formation of quadruplets is highly favourable for Sn adatoms. Moreover, the observation of single dots at very low Sn coverages that are composed by 4 Sn atoms suggests that individual Sn quadruplets form on Cu(001) at LT. Pointing in the same direction is the fact that Sn quadruplets were also proposed as a building block of the $c(4 \times 4)$ reconstruction of the Sn/Cu(001) formed at RT [17,19].

With increasing temperature the process of detachment from the LT structures is activated generating higher-size islands at ~200 K, whereas the exchange process is already present but with low probability. At ~240 K the exchange process is more probable and all the non-alloyed surface reconstructions transform into the known alloyed structures observed at RT. At very low coverages we see the formation of small rectangular islands, identified as (2×2) alloy structures, surrounded by embedded Sn atoms. These (2×2) alloy islands would be metastable as they are not present when depositing at RT. Remarkably, these (2×2) structures show a rather narrow distribution in size around the typical squared domains that form the $p(2 \times 2)$ reconstruction. The fact that the (2×2) surface alloy forms at low coverages strongly suggests that it is the most favourable ordered structure among the observed reconstructions. However, most of these (2×2) islands do not growth beyond the size of (4×4) Sn atoms, due to the increase of the elastic energy. This explains the origin of the domain walls in the $p(2 \times 2)$ surface alloy reconstruction formed at RT.

Another relevant conclusion derived from the STM and LEED experiments is that the five ordered phases formed by the system at RT (namely $p(2 \times 2)$, $p(2 \times 6)$, $c(4 \times 8)$, $(3\sqrt{2} \times \sqrt{2})R45^{\circ}$ and $c(4 \times 4)$), can be obtained starting from the LT non-alloying phases and increasing the temperature. Moreover, there are no other reconstructions at intermediate temperatures. From LEED experiments, we found that all the transitions occur in the same temperature range (which from the STM experiments is determined to be between 200 and 240 K) when the exchange process is activated.

Acknowledgements

We acknowledge financial support from CONICET (PIP-2015-00274), ANPCYT (PICT-2015-0922), and UNCuyo (06/C498). We thank O. Grizzi for fruitful discussions.

References

[1] J. Rodriguez, Physical and chemical properties of bimetallic surfaces, Surf. Sci. Rep. 24 (7–8) (1996) 223–287.
[2] A. Christensen, A.V. Ruban, P. Stoltze, K.W. Jacobsen, H.L. Skriver, J.K. Nørskov, F. Besenbacher, Phase diagrams for surface alloys, Phys. Rev. B 56 (1997) 5822–5834.
[3] D. Woodruff, E. Vlieg, Chapter 8 – The structure of surface alloy phases on metallic substrates, in: D. Woodruff (Ed.), Surface Alloys and Alloys Surfaces. The Chemical Physics of Solid Surfaces, vol. 10, Elsevier, 2002, pp. 277–304.
[4] J.G. Chen, C.A. Menning, M.B. Zellner, Monolayer bimetallic surfaces: experimental and theoretical studies of trends in electronic and chemical properties, Surf. Sci. Rep. 63 (5) (2008) 201–254.
[5] A.F. Lee, C.J. Baddeley, C. Hardacre, G.D. Moggridge, R.M. Ormerod, R.M. Lambert, J.P. Candy, J.-M. Basset, Structure-reactivity correlations in the catalytic coupling of ethyne over novel bimetallic Pd/Sn catalysts, J. Phys. Chem. B 101 (15) (1997) 2797–2805.
[6] F. Studt, M. Behrens, E.L. Kunkes, N. Thomas, S. Zander, A. Tarasov, J. Schumann, E. Frei, J.B. Varley, F. Abild-Pedersen, J.K. Nørskov, R. Schlgl, The mechanism of CO and CO_2 hydrogenation to methanol over Cu-based catalysts, ChemCatChem 7 (7) (2015) 1105–1111.
[7] A. Carrera, L.J. Cristina, S. Bengi, A. Cossaro, A. Verdini, L. Floreano, J.D. Fuhr, J.E. Gayone, H. Ascolani, Controlling carboxyl deprotonation on Cu(001) by surface Sn alloying, J. Phys. Chem. C 117 (33) (2013) 17058–17065, http://dx.doi.org/10.1021/jp404983n.
[8] Helicenes: from random structures to dense racemic crystals by surface alloying.
[9] G.L. Kellogg, Chapter 5 – Surface alloying and de-alloying of Pb on single-crystal Cu surfaces, in: D. Woodruff (Ed.), Surface Alloys and Alloys Surfaces, The Chemical Physics of Solid Surfaces, vol. 10, Elsevier, 2002, pp. 152–183.
[10] S. Karakalos, S. Kennou, S. Ladas, P. Janecek, F. Sutara, V. Nehasil, S. Fabik, N. Tsud, K. Prince, V. Matolin, V. Chab, The transition from the adsorbed state to a surface alloy in the Sn/Ni(111) system, Surf. Sci. 600 (18) (2006) 4067–4071, Proceedings of the 23th European Conference on Surface Science, Berlin, Germany, 4–9 September 2005.
[11] X. Liang, J.-H. Deng, L.-J. Fan, Y.-W. Yang, D.-A. Luh, Nonalloying surface reconstructions of ultrathin Sn films on Cu(111) investigated with LEED, XPS, and photoelectron extended fine structure analysis, Phys. Rev. B 84 (2011) 075406.
[12] E. McLoughlin, A. Cafolla, E. AlShamaileh, C. Barnes, A re-interpretation of the Cu(100)/Sn surface phase diagram, Surf. Sci. 482–485 (Part 2) (2001) 1431–1439.
[13] A. Cafolla, E. McLoughlin, E. AlShamaileh, P. Guaino, G. Sheerin, D. Carty, T. McEvoy, C. Barnes, V. Dhanak, A. Santoni, Observation of an anti-phase domain structure in the Cu100/Sn surface alloy system, Surf. Sci. 544 (2003) 121–133.
[14] K. Pussi, E. AlShamaileh, E. McLoughlin, A. Cafolla, M. Lindroos, Determination of the structure of Cu100-p(322)R45°-Sn by dynamical {LEED}, Surf. Sci. 549 (1) (2004) 24–30.
[15] J. Martínez-Blanco, V. Joco, T. Balasubramanian, P. Segovia, E.G. Michel, Surface phase diagram and temperature induced phase transitions of Sn/Cu(001), Appl. Surf. Sci. 252 (2006) 5331.
[16] Y. Nara, K. Yaji, T. Iimori, K. Nakatsuji, F. Komori, STM observation of surface phases of Sn/Cu(001), Surf. Sci. 601 (22) (2007) 5170–5172, Proceedings of the 10th {ISSP} International Symposium on Nanoscience at Surfaces ISSP 10.
[17] J. Lallo, L. Goncharova, B. Hinch, S. Rangan, R. Bartynski, D. Strongin, Structural studies of sub monolayer Sn/Cu(001) structures, Surf. Sci. 602 (14) (2008) 2348–2357.
[18] J.D. Fuhr, J.E. Gayone, J. Martínez-Blanco, E.G. Michel, H. Ascolani, Structural and electronic properties of $\left(3\sqrt{2}\mathrm{x}\sqrt{2}\right)$R45°-Sn/Cu(100): a DFT and STM study, Phys. Rev. B 80 (2009) 115410.
[19] K. Yaji, R. Nakayama, K. Nakatsuji, T. Iimori, F. Komori, Ordered structures of tin-adsorbed Cu(001) surfaces with over monolayer coverage, Surf. Sci. 603 (2) (2009) 341–348.
[20] P. Giannozzi, S. Baroni, N. Bonini, M. Calandra, R. Car, C. Cavazzoni, D. Ceresoli, G.L. Chiarotti, M. Cococcioni, I. Dabo, et al., QUANTUM ESPRESSO: a modular and open-source software project for quantum simulations of materials, J. Phys.: Condens. Matter 21 (2009) 395502.
[21] J.P. Perdew, K. Burke, M. Ernzerhof, Generalized gradient approximation made simple, Phys. Rev. Lett. 77 (1996) 3865–3868.
[22] J.P. Perdew, K. Burke, M. Ernzerhof, Generalized gradient approximation made simple [Phys. Rev. Lett. 77, 3865 (1996)], Phys. Rev. Lett. 78 (1997), 1396–1396.
[23] J. Tersoff, D.R. Hamann, Theory of scanning tunneling microscope, Phys. Rev. B 31 (1985) 805–813.
[24] R. van Gastel, E. Somfai, S.B. van Albada, W. van Saarloos, J.W.M. Frenken, Nothing moves a surface: vacancy mediated surface diffusion, Phys. Rev. Lett. 86 (2001) 1562–1565.
[25] M.L. Grant, B.S. Swartzentruber, N.C. Bartelt, J.B. Hannon, Diffusion kinetics in the Pd/Cu(001) surface alloy, Phys. Rev. Lett. 86 (2001) 4588–4591.
[26] M. Anderson, N. Bartelt, B. Swartzentruber, The importance of Pb-vacancy attractions on diffusion in the Pb/Cu(001) surface alloy, Surf. Sci. 538 (1–2) (2003) 53–58.
[27] While it is well-known that multiple scattering (or so-called dynamical theory) is essential to describe the energy dependence of LEED beam intensities, it is also known that the average relative intensities of the beams (i.e., the appearance of the LEED pattern) can be quite effectively simulated by a single scattering description.
[28] We note that the graph in panel (c) shows the intensity of the (1/2,1/2) spot together with a given $c(4 \times 4)$ spot as a function of time. Although the (1/2,1/2) spot is present in both the non-alloy and the alloy structures, it was chosen because the other fractionary spots of the $c(4\sqrt{2} \times 2\sqrt{2})R45^{\circ}$ pattern are too weak to be followed.